ELF receiver for magnetic field: frequency response characterization and natural signals detection

W. G. Fano[†1], L. M. Carducci [†2] and R. Alonso[†3]

[†] *Universidad de Buenos Aires, Facultad de Ingeniería,*
Laboratorio de Radiación Electromagnética - Laboratorio de Procesamiento de Señales y Comunicaciones
Paseo Colón 850. (1063) Buenos Aires. Argentina
[1]gfano@fi.uba.ar
[2]lcarducci@fi.uba.ar
[3]ralonso@fi.uba.ar

***Abstract*—This article presents an antenna design and characterisation of a system to measure extremely low frequencies magnetic fields signals. To improve its sensitivity, the antenna is made with a considerably high inductance coil and then connected to a high gain amplification system. The antenna impedance was measured by mean of a LCR meter, in the 3-187 Hz rank. Then a realistic circuit model that includes parasitic effects was determined, which are relevant because the antenna has a very low resonance frequency. The signals are digitized and stored using an autonomous acquisition system at a 100 Hz sampling frequency. Due to possible aliasing effects, a frequency domain analysis was performed to determine the performance of the antenna-amplifier assembly. The characteristics of the sensor were defined for measuring and studying extremely low frequencies naturals signals, considering electromagnetic fields emissions that are present on the earth surface all times. For example, solar emissions, volcanic eruptions, earthquakes precursors and galactic noise. A particular case which has been tested was the measurement of the Schumann resonances, a very weak and low frequency natural magnetic waves that occurs between earth surface and ionosphere.**

***Index Terms*—Loop antenna, ELF, Magnetic fields, acquisition system, Schumann Resonance**

I. Introduction

Electromagnetic Fields are present on the Earth surface, due to natural and artificial emissions. The Earth's magnetic field is not only static, also includes very slow time variations: secular, annual, 27 days, diurnal and substorm magnetic bay type variations at very low frequency (<1 mHz).The geomagnetic pulsations phenomena, take place from 1 mHz to 1 Hz. This is generated by the solar wind interacting with the magnetosphere. During the past few decades, a remarkable increase in the quality and quantity of electromagnetic data recorded before and during eruptions and earthquakes [1] are evidence that seismic movements are preceded by anomalous electromagnetic signals. The Electromagnetic earthquake precursors signals have been discussed in many publications and are also studied in our research project [2], [3]. Aspects of tectonomagnetism, volcanomagnetism and tectonoelectricity, concentrate on various parts of the electromagnetic spectrum from radio frequencies (RF) to submicrohertz frequencies [1]. Other electromagnetic phenomena in the ULF/ELF band are originated by particles impinging on the magnetosphere causing electromagnetic emissions that propagate inside the magnetosphere cavity [4]. Lightning flashes are the main source of energy for the electromagnetic background inside the ionospheric cavity. Starting from the lower band ELF (few Hz) up to VHF (hundreds MHz) the noise originates mainly from the energy radiated by lightning strokes. The main relevant phenomena in the ELF lower band are the *Schumann Resonances* (SR) [4]. The Earth and the ionospheric layers appear as perfect conductors having air in between, forming an Earth-ionosphere cavity, in which electromagnetic radiation is trapped. Lightning strikes within the troposphere radiate energy into this system and the waves travel around the Earth. In the case of constructive interference, Earth-ionosphere cavity resonances are excited [4]. The SR oscillation detection is a complex procedure which requires customized and high-quality measurement systems. The detection of SR employs the limited energy generated and dissipated by the global lighting activity. The magnetic field amplitudes received are about few tenths of pico Tesla. [5]. The most important naturally occurring VLF signal is the whistler. A whistler is created from a lightning stroke that passes first to the ionosphere and then to the magnetosphere above. These particles are then guided along the Earth's magnetic field, returning to ground to the opposite hemisphere [2].

The study of these very low frequencies electromagnetic phenomena mentioned above, has motivated the construction of a specific acquisition system for this electromagnetic spectrum range. The main objective of this work is focused on the characterization of a high-sensitivity antenna used as a sensor for magnetic waves in the ELF band and the system performance as a whole. In the section II a circuit model for the antenna used is proposed. The section III describes the main system specifications, including the antenna, a high-gain amplifier and the digitizing system. Then, the section IV shows the results obtained in the antenna model parameters characterization, the complete system transference and the Schumann resonances measured in filed test. Finally, in sections V and VI the general conclusions and some aspects that are expected to be carried out in the near future are mentioned.

II. Antenna Modeling

A. Proposed design

For the applications of interest mentioned in this work, the design, implementation and modeling of a high inductance loop antenna with magnetic core is proposed. The chosen design diagram can be seen in the Figure 1. This antenna consists of eight commercial copper windings with a large number of turns each, connected in series around a high permeability core. This configuration was chosen to have a simpler and more practical assembly. On the other hand, a plastic cover was also incorporated for protection. In later sections more details and characteristics will be seen.

B. Equivalent Circuit Model

The proposed antenna is essentially an inductor, which can be represented as an ideal inductance L. Thus, the simple model for impedance of the antenna results $Z(\omega) = j\omega L$. However, a series resistance R_s must be included due to wire losses, obtaining $Z(\omega) = j\omega L + R_s$. On the other hand, due to the high inductance for this antenna design, a considerably low resonant frequency occurs, therefore capacitive effect must also be taken into account. Then, an improvement of the model contemplates an equivalent parasitic capacity C which is caused by the copper winding. In this case would be $Z(\omega) = (j\omega L + R_s)//(j\omega C)^{-1}$. Finally, others losses represented as an equivalent resistance in parallel R_p to the whole assembly can also be considered, that is $Z(\omega) = (j\omega L + R_s)//(j\omega C)^{-1}//R_p$. In this way, in Figure 2 the definitive circuit model proposed for the loop antenna with a magnetic core is shown. Likewise, the total impedance can also be rewritten as a function of their active and reactive parts: $Z(\omega) = R(\omega) + jX(\omega)$. In Equations 1 and 2, both parts are expressed in terms of all electrical parameters and the angular frequency.

$$R(\omega) = \frac{\left(R_s + \frac{R_s^2}{R_p} + \omega^2 \frac{L^2}{R_p}\right)}{\left(1 - \omega^2 LC + \frac{R_s}{R_p}\right)^2 + \left(\omega \frac{L}{R_p} + \omega R_s C\right)^2} \quad (1)$$

$$X(\omega) = \frac{\left(\omega L - \omega^3 L^2 C - \omega R_s^2 C\right)}{\left(1 - \omega^2 LC + \frac{R_s}{R_p}\right)^2 + \left(\omega \frac{L}{R_p} + \omega R_s C\right)^2} \quad (2)$$

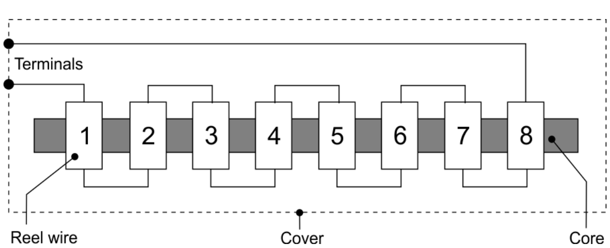

Fig. 1. Design of the proposed loop antenna.

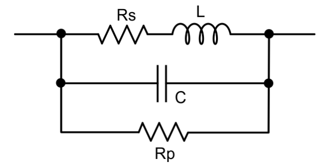

Fig. 2. Equivalent electric circuit of the receiver antenna: ideal inductance L; series resistance R_s; parasitic capacity C; parallel loss resistance R_p.

III. Materials and Specifications

This section describes some characteristics and specifications for different components and main stages for a low frequency magnetic field measurement system. In Figure 3 the sensing system simplified scheme can be seen. It includes the following stages: *loop antenna*, *high gain amplifier + filter*, and *digital acquisition*. These are briefly described below.

A. Antenna Specifications

An iron core loop antenna with a square section and a large number of wire turns has been built. The antenna is made up of 8 reels of copper wire, as can be seen in Figure 1, with around 12000 turns each, obtaining a total 96000 turns. In Table I its main design parameters are detailed. Likewise, in Figure 4 a picture with different parts of the built antenna can be seen. A feature to highlight is the huge number of turns and relatively high core permeability, since this implies a very high inductance which improve its sensitivity for detecting very weak magnetic field signals at very low frequencies.

TABLE I
LOOP ANTENNA SPECIFICATIONS

Parameter	Specification
Core section	rectangular
Side (m)	$0,0285$
Core area (m^2)	$9 \cdot 10^{-4}$
Wire radius (mm)	$0,12$
Wire resistance ($k\Omega$)	18,6
Number of turns (total)	96000
μ_r (approx.)	35
Resonant frequency (Hz)	200

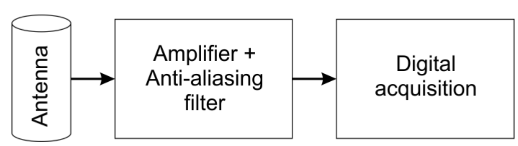

Fig. 3. Stages of the magnetic field measurement system.

Fig. 4. Loop antenna (high sensitivity). (a) eight reels on core; (b) a single reel; (c) cover protection and antenna connector.

B. High Gain Amplifier and Anti-aliasing Filter

The voltage induced in the coil (close to micro-volt), is amplified by a high gain amplifier (*Minimum Open Loop Amplifier*, MOLA) [6] of up to $G_0[\text{dB}] \simeq 88$ dB, with a very low common mode rejection ratio. An anti-alising filter is also included to mitigate the signals of 50 Hz interference due to the public electric service and other higher frequency components. It should be noted that in Villa Alpina the closest public power grid is 8 km away, which reduces the presence of this type of interference [6]. Even so, the equipment grounding scheme was carefully planed, with all ground references connected to the metal chassis of the testing equipment. All the system was powered by a 12V/ 75Ah battery and ± 9 V voltage regulators. The amplifier input resistance has been set at $R_{in} = 39\,\text{k}\Omega$ and the output resistance at $R_o = 1,2\,\text{k}\Omega$. For the anti-aliasing filter two capacitors were connected in parallel $4,7\,\mu\text{F}//470\,\text{nF}$ to the amplifier output. This result in a total capacity $C_o \simeq 5,17\,\mu\text{F}$, forming a simple first order low pass filter, whose theoretical cut-off frequency is $f_c = (2\pi R_o C_o)^{-1} \simeq 25$ Hz. Later, a more detailed analysis about this aspect will be developed.

C. Data Acquisition System

At the amplifier output, the amplified signal is digitized by an analog to digital converter (ADC) with 12-bit resolution and sample rate 100 Hz. The input resistance R_D for this ADC is considered much bigger than amplifier resistance output, that is $R_D >> R_o$. The acquired data are encoded and stored in an 8 GB micro-SD memory, storing one minute long data for each file, also including additional information as date, time, and other variables detected. For this digital part, a 32-bit microcontroller cortex-M3 LPC1769 is used. All parts of the measurement system has been installed inside a metal cabinet located inside a waterproof plastic enclosure.

IV. Methods and Experimental Results

A. Measurement and fit model of the antenna

The electrical circuit of the loop antenna have been measured by mean of an LCR meter for frequencies between 12 Hz and 187 Hz. For measuring lower frequencies (< 12 Hz) a setup with an Oscilloscope and a function generator was used. All results can be observed in the Table III. The typical inductive behaviour of the loop antenna is depicted in the measurement of the reactance $X(\omega) = \Im m\{Z(\omega)\}$ versus the frequency, as can be observed in the Figure 5. In this graph, the reactance can be approximated as a constant slope line for low frequencies thus noticing its inductive behaviour, but changing this trend when the frequency approaches resonance. As for the real part, $R(\omega) = \Re e\{Z(\omega)\}$, it increases with the frequency due to the Joule effect in a conductor and the losses in the magnetic core, as can be seen in Figure 6. The estimated curves for the antenna model (dotted lines) are displayed using the best-fitting model to measured data. Parameters values for this model were determined in different ways. The series resistance $R_s = 18,6$ kΩ was measured directly at DC. The inductance was deduced by computing the slope of the reactance at low frequencies adding a posterior numerical adjustment, resulting in a value close to $L \simeq 800$ H. Likewise, there is a stray capacitance due to the layers of the loop antenna windings. Therefore, due to stray capacitance and huge inductance, a resonance at unusually low frequencies was observed, resulting $f_0 \simeq 200$ Hz. Then, for resonance condition ($X(\omega) = 0$ in Eq. 2) the stray capacitance is $C = 0,79$ nF which can be determined by $C = L/(\omega_0^2 L^2 - R_s^2)$. Last, the parallel resistance was estimated using numerical approximations to fit model, obtaining $R_p = 1,89$ MΩ.

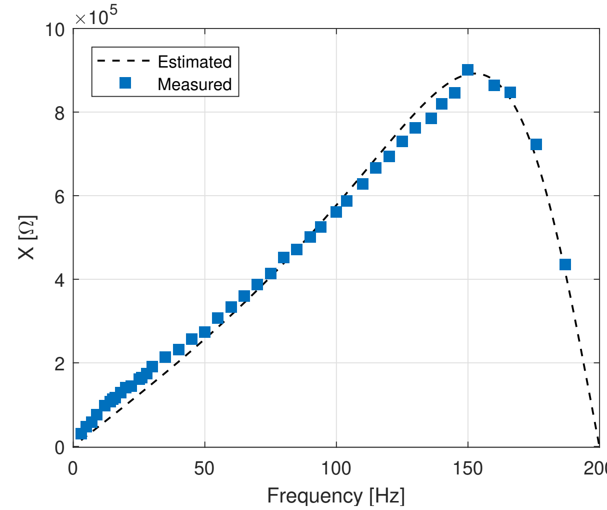

Fig. 5. Imaginary part of the antenna impedance (estimated and measured).

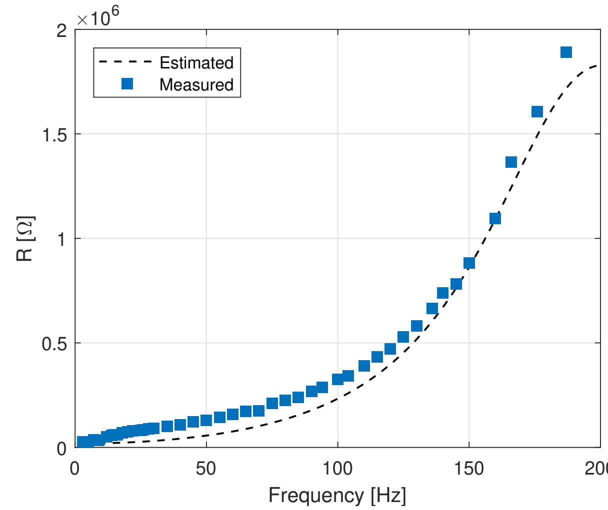

Fig. 6. Real part of the antenna impedance (estimated and measured).

B. Attenuation at the antenna-amplifier interface

In Figure 7 the simplified electrical circuit which describes the connection between antenna and amplifier is shown. There, the induced voltage V_{oc} which occurs when a magnetic field is present, is connected in series with the antenna impedance itself $Z(\omega)$. The resulting effect is a frequency dependent attenuation at the input interface represented by R_{in}. Considering this situation, the Eq. 3 defines the attenuation $A(\omega)$ as the relationship between open circuit voltage $V_{oc}(\omega)$ and input voltage of the amplifier $V_{in}(\omega)$. Here, the antenna impedance and amplifier input resistance produce a significantly loading effect for the useful frequency range (0-50 Hz) due the antenna inductance which is unusually high. This could lead to the conclusion that the problem would be solved by increasing the amplifier input resistance. However, as will be seen later, other conclusions can be obtained by doing a more detailed analysis. In Figure 8 multiple possible curves for the attenuation $|A(\omega)|$ are shown. In solid blue lines attenuations parameterized with different hypothetical values for the input resistance of the amplifier R_{in} can be seen. Looking this attenuation in isolation, can be seen that if the input resistance were high (eg. $R_{in} = 3.9$ MΩ) the attenuation would be low, while for a low resistance (eg. $R_{in} = 680$ Ω) the attenuation would be considerably higher around the resonance. There, $|A(\omega)|$ (in black dotted line) can also be seen, but for the true input resistance $R_{in} = 39$ kΩ in the implemented amplifier. However, a whole analysis that includes the amplification stage is necessary to reach a better conclusion where the aliasing effects are also considered.

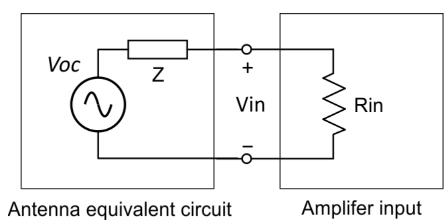

Fig. 7. Connection between the antenna equivalent circuit (induced voltage $V_{oc}(\omega)$ and antenna impedance $Z(\omega)$) and amplifier input resistance R_{in}.

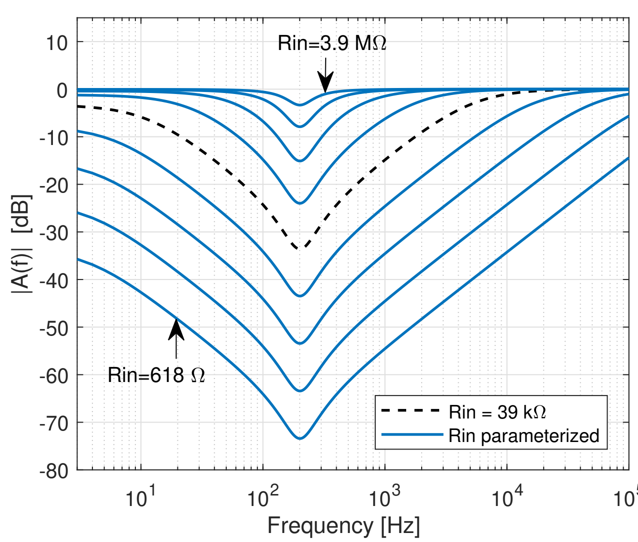

Fig. 8. Input attenuation $|A(f)|$ parameterized with R_{in}, for hypothetical values (solid blue lines) and true (black dotted lines).

$$A(\omega) = \frac{V_{in}(\omega)}{V_{oc}(\omega)} = \frac{R_{in}}{R_{in} + Z(\omega)} \tag{3}$$

C. Amplifier and filter transference

Considering the equivalent circuit and the voltages indicated in Figure 9, the transfer $V_{out}(\omega)/V_{in}(\omega)$ can be defined as expressed in Eq. 4, where $V_{in}(\omega)$ and $V_{out}(\omega)$ are the amplifier input and output voltages, respectively. In Figure 10 the theoretical and measured frequency response magnitude can be seen, showing a cutoff frequency close to $f_c = 25$ Hz and a maximum gain around $G_0|_{\text{dB}} = 88$ dB.

$$G(\omega) = \frac{V_{out}(\omega)}{V_{in}(\omega)} = \frac{G_0}{1 + j\omega R_o C_o} \tag{4}$$

D. Full transference and induced voltage

The total transference $T(\omega)$ relates $V_{out}(\omega)$ with $V_{oc}(\omega)$ and is defined as the product between attenuation and amplification stages. That is $T(\omega) = A(\omega)G(\omega)$, resulting in Eq. 5.

$$T(\omega) = \frac{V_{out}(\omega)}{V_{oc}(\omega)} = \frac{R_{in}}{R_{in} + Z(\omega)} \, \frac{G_0}{1 + j\omega R_o C_o} \tag{5}$$

Analogously to the curves shown for $A(\omega)$, in Figure 11 the frequency response modulus $|T(\omega)|$ parameterized with R_{in}

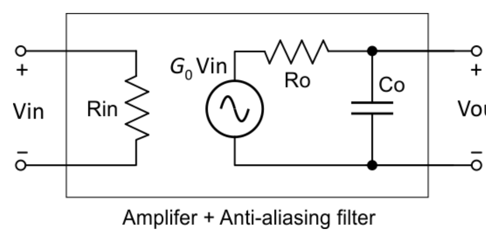

Fig. 9. Amplifier equivalent circuit, where R_{in} is the input impedance, G_0 is the maximum gain, R_o the output resistance and C_o the output capacitance.

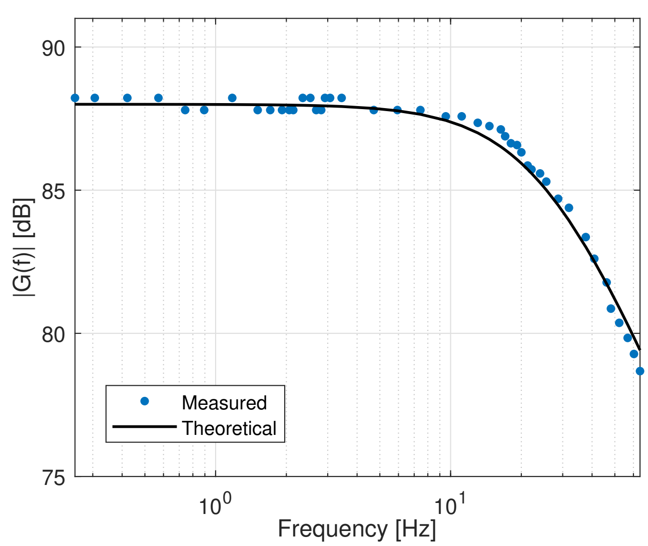

Fig. 10. Frequency response of the amplifier transference $|G(f)|$.

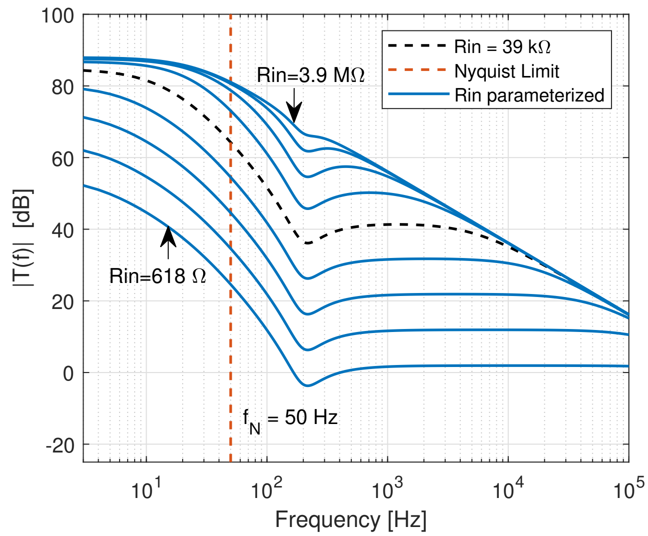

Fig. 11. Total transference $|T(f)|$ parameterized with R_{in}, for hypothetical values (solid blue lines) and true (black dotted lines).

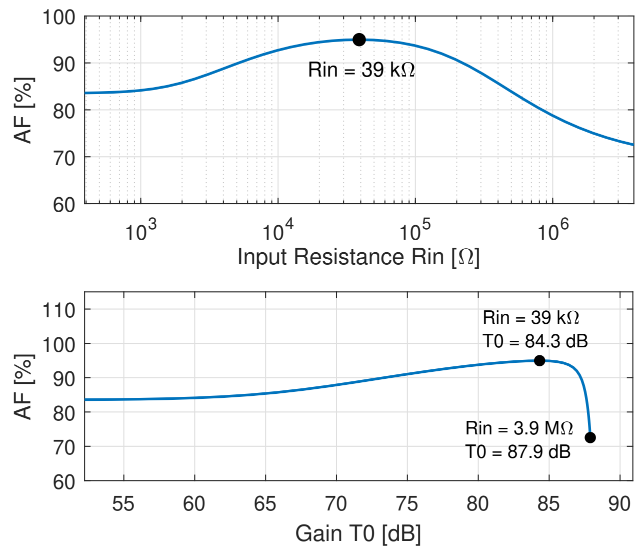

Fig. 12. AF[%] as function of input resistance R_{in} (above) and as function of DC gain $T_0|_{\text{dB}}$ (below).

is plotted. There, it can be observed the transference curve for $R_{in} = 39$ kΩ (dotted black line). Also, it is shown that when R_{in} is big, the transference is close to $G(\omega)$, but when R_{in} is small the behavior is notoriously different.

There are two relevant aspects to define how optimal the measurement system is for the proposed antenna. First, it's important to analyze the gain of the complete system, since the attenuation $A(\omega)$ can significantly reduce the gain provided by the amplifier. This is relevant because the higher gain is, the better the system sensitivity becomes. Second, the digital acquisition device has a sampling rate of $f_s = 100$ Hz. This implies a limit on the available spectrum given by the Nyquist frequency, which in this case is $f_N = 50$ Hz. Therefore, to avoid a possible aliasing effect, it's necessary that the frequency behavior of $T(\omega)$ maximizes the energy in the useful band (0-50 Hz) and minimizes it in the non-useful band (50-∞ Hz). From Figure 11, is important to observe that for low R_{in} the energy in the non-useful range seems to have a better rejection of aliasing although with a large gain reduction, while that for high R_{in}, the gain is significantly higher although with a poor behavior against aliasing. To quantify this condition, the quotient between the filter energy in the useful range ($0 \leq \omega < \omega_N$) and the total energy for all range ($0 \leq \omega < +\infty$) can be defined as a merit factor. In this way, the *Anialiasing Factor* (AF) can be expressed as indicated in the equation 6, where $\omega_N = 2\pi 50$ [rad/s] is the Nyquist angular frequency.

$$AF = \frac{\int_0^{\omega_N} |T(\omega)|^2 d\omega}{\int_0^{+\infty} |T(\omega)|^2 d\omega} \tag{6}$$

From this definition, it is possible to analyze the performance of the antialiasing filter by evaluating AF based on the different hypothetical values of R_{in}. In the Figure 12 this function (expressed in percentage [%]) can be seen, observing that for both low and high values of R_{in} the filter behavior is worse for aliasing filtering, while the optimal value that maximizes AF is given for $R_{in} \simeq 39$ kΩ.

On the other hand, since it's also important to analyze the total system gain, AF can be plotted in function of a reference gain corresponding for each value of R_{in}. In this case, the DC gain $T_0 = |T(0)|$ has been chosen. Then, according to Figure 12, AF decreases significantly as T_0 approaches the maximum possible value, that is 88 dB, which is precisely when $R_{in} \to \infty$. It is also noticeable that for the optimal case ($R_{in} = 39$ kΩ) the gain is $T_0 = 84,3$ dB, maintaining a gain relatively close to maximum. However, for a future design, the gain could be increased by slightly increasing R_{in} for a sub-optimal but close to maximum AF value.

Knowing then the total analog stage transference, it's possible to obtain the induced voltage $V_{oc}(\omega)$ computing the spectrum of signal $v_{out}(t)$ which is sampled by the acquisition system. To do this, the spectrum $V_{out}(\omega)$ can be equalized by applying the inverse of $T(\omega)$ to obtain then $V_{oc}(\omega)$. In Figure 13, the total transfer (blue solid and black dotted lines) and the equalization function $|T(\omega)|^{-1}$ (black solid line) are plotted. It is important to clarify that for a more general case, this type of equalization can have instability problems if there are zeros located outside left half plane in Laplace's s space, or also noise amplification at high frequencies. Regarding instability, in the presented system there is no such problem since the $T(s)$ only has one pole in the left half plane, so its inverse doesn't have any pole. On the other hand, although there is noise amplification, the useful spectrum for signal is relatively low for 100 Hz sample rate and the noise amplification can be mitigated by subsequent processing techniques. Then, according to Eq. 7 the compensated spectrum magnitude $|V_{oc}(\omega)|$ can be determined.

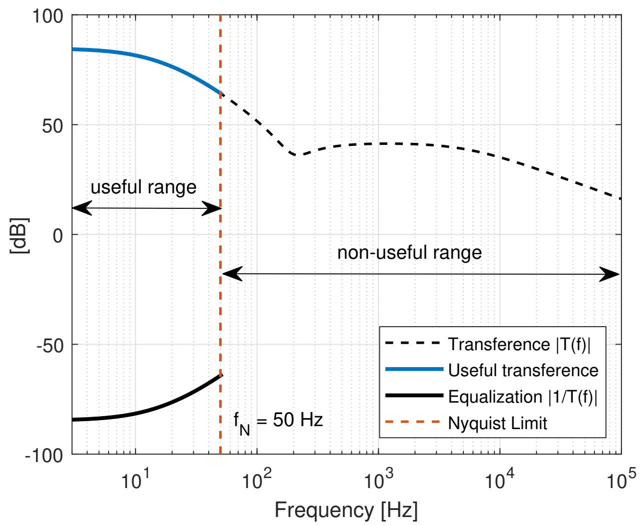

Fig. 13. Total transference $|T(f)|$ and $|T(f)|^{-1}$ for $R_{in} = 39$ kΩ.

$$|V_{oc}(\omega)| = \frac{|Z(\omega) + R_{in}| \sqrt{1 + (\omega R_o C_o)^2}}{G_0 R_{in}} |V_{out}(\omega)| \quad (7)$$

E. Experimental application: Schumann resonances detection

Taking into account the objectives of this work, it's important to verify how effective the proposed antenna is in conjunction with the rest of system to detect very small natural electromagnetic signals. In this case, the authors have measured the Schumann resonances in the location of Villa Alpina, Córdoba, Argentina. Figure 14 shows the complete installation of the sensor station on site, which has also been used in other works with similar antennas [7], [6]. This location was chosen due to the very low artificial noise of the power lines radiation and others possible urban interference of higher frequencies [8]. In order to see the spectrum of the amplifier output signal, the power spectral density (PSD), $S_{out}(\omega)$ [V^2/Hz], it can be calculated from digitized and stored data. For the better plotted and visibility of the Schumann Resonances peaks, the average PSD can be used, according to some methods seen in [7]. Then, the amplifier output voltage spectrum can be computed as $|V_{out}(\omega)| = S_{out}^{1/2}(\omega)$ [V/$\sqrt{\mathrm{Hz}}$]. This is shown in Figure 15. There up to the first seven Schumann resonances can be clearly seen. Table II summarizes the mean and deviation of the frequencies estimated using 60 PSDs of one minute long each. Finally, the induced voltage spectrum modulus $|V_{oc}(\omega)|$ can be calculated by mean of the equation 7 and using the estimation of $|V_{out}(\omega)|$, thus obtaining the graph of Figure 16. There is noticeable an increase in the amplitude as the frequency increases, but this feature is normal, as can be seen in similar works such as [9]. Likewise, the last stage in the estimation, which is not part of this work, would be to apply the antenna factor to obtain the spectrum measured in units of magnetic field (tesla), that is $B(\omega) = K(\omega)\, V_{oc}(\omega)$. The antenna factor K tends to be an inversely proportional to the frequency, so the noise floor would be approximately flat after applying it.

Fig. 14. Installation of the Sensing Station and the antenna in Villa María, Córdoba, Argentina.

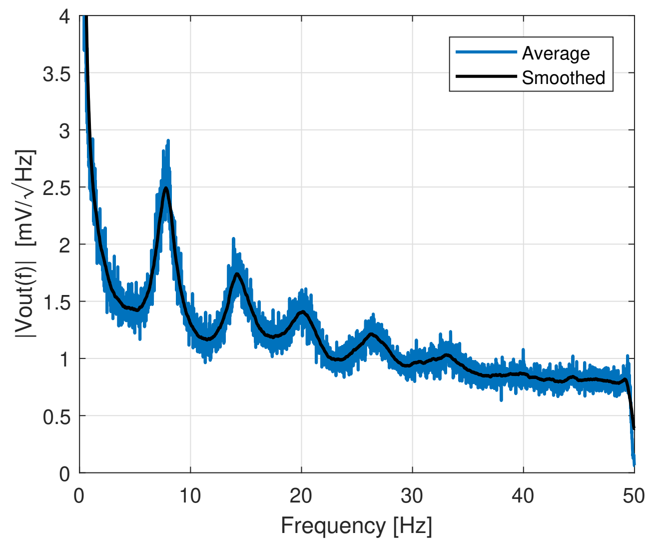

Fig. 15. Average PSD of the voltage measured (60 time windows of one minute each) and smoothed curve. An additional digital filter has also been applied to suppress 50 Hz components.

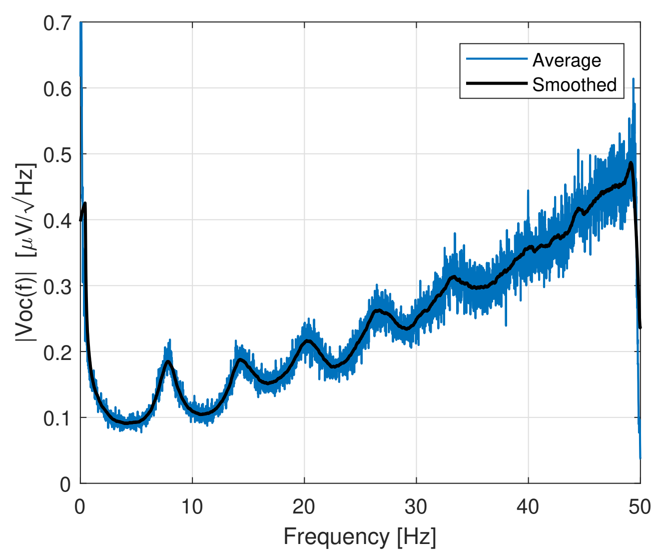

Fig. 16. Average PSD and smoothed curve of the voltage induced estimated.

TABLE II
SCHUMANN RESONANCES ESTIMATED FROM MEASUREMENTS

Parameter	1st	2nd	3rd	4th	5th	6th
Mean [Hz]	7.84	14.23	20.67	26.67	32.53	39.83
Deviation [Hz]	0.10	0.09	0.14	0.14	0.18	0.19

TABLE III
MEASUREMENT OF THE LOOP ANTENNA WITH MAGNETIC CORE.

F [Hz]	X $[k\Omega]$	R $[k\Omega]$	F [Hz]	X $[k\Omega]$	R $[k\Omega]$
3	30,29	26,34	70	387,04	175,93
5	47,25	25,4	75	414,22	211,34
7	57,44	35,68	80	452,39	226,19
9	75,55	33,73	85	471,05	239,11
12	97,26	51,46	90	501,02	267,93
14	107,4	57,44	94	525,65	287,24
15	113,47	59,72	100	560,46	325,85
16	116,62	60,42	104	587,45	341,54
18	128,48	69,07	110	627,56	389,79
20	140,12	73,74	115	666,21	432,6
22	144,31	78,86	120	694,42	472,39
25	161,01	82,57	125	730,42	529,29
26	164,67	83,59	130	762,01	581,68
28	174,7	89,59	136	785,3	665,51
30	190,38	90,66	140	819,83	738,59
35	213,31	101,58	145	845,47	782,84
40	231,72	108,79	150	901,01	883,34
45	257,01	122,39	160	864,57	1094,39
50	273,32	130,15	166	846,92	1366,01
55	307,22	143,56	176	723,22	1607,16
60	332,88	158,82	187	434,73	1890,15
65	359,4	171,47	-	-	-

V. CONCLUSIONS

In this work has characterized a loop antenna at very low frequencies to determinate its equivalent impedance model. Also, numeric approximations to estimate other parameters of the model have been used. With these result, a huge inductance $L \simeq 800$ H has been verified, which implies a very high sensibility for field sensing. An unusually low frequency of resonance, near to 200 Hz, was observed due to the huge inductance and the parallel stray capacitance. It was found that the proposed antenna together with the rest of the measurement system have a very good performance in the range of frequencies of interest. This is verified by analyzing the total transfer of the analog measurement stage, observing an optimal behavior for aliasing filtering and guaranteeing a high gain. The resulting portable equipment shown a very high sensitivity, prooving it can detect very weak natural signals at extremely low frequencies. As a particular application case the first six Schumann resonances have been detected successfully and with great precision.

VI. FUTURE WORKS

It is expected to measure antenna factor to determinate the magnetic filed B (*tesla*) from voltage measured. To do this, a measurement bench with Helmholtz coils of a suitable size will be used to generate a known magnetic field as a calibration reference. Likewise, tests will be carried out with other magnetic materials and also assembly three antennas that allow monitoring the three spatial components of the near field.

VII. ACKNOWLEDGMENT

The authors would like to thank to Edgardo Maffia from Electronica Aplicada Company for the help during experimental process. To Norman Trench for taking care of the installation of equipment and the magnetic field measurements. To the Universidad de Buenos Aires for the project Grant 20020150100085.

REFERENCES

[1] M. J. S. JOHNSTON, “Review of electric and magnetic fields accompanying seismic and volcanic activity,” *Surveys in Geophysics*, vol. 18, no. 5, p. 441–475, 1997.

[2] W. G. Fano, G. Quintana, and R. Alonso, “3D magnetic field measurement at ELF and SLF frequencies,” *IEEE 2018 GEMCCON*, 2018.

[3] G. I. Quintana, R. Alonso, and W. G. Fano, “Loop antenna characterization for ELF and SLF measurements,” *Elektron, Universidad de Buenos Aires, Argentina.*, vol. 2, no. 2, p. 95–100, 2018.

[4] C. Bianchi and A. Meloni, “Loop antenna characterization for ELF and SLF measurements,” *ANNALS OF GEOPHYSICS.*, vol. 50, no. 3, p. 435–445, 2007.

[5] C. I. Votis, G. Tatsis, V. Christofilakis, S. K. Chronopoulos, P. Kostarakis, V. Tritakis, and C. Repapis, “A new portable ELF Schumann resonance receiver: design and detailed analysis of the antenna and the analog front-end,” *EURASIP J. Wirel. Commun. Netw.*, vol. 2018, p. 155, 2018. [Online]. Available: https://doi.org/10.1186/s13638-018-1157-7

[6] N. Trench, R. Alonso, L. M. Carducci, J. Kelly, E. Maffia, E. Zothner, J. Zola, and W. G. Fano, “Sistema de medición remota de campo magnético para señales precursoras sísmicas de muy bajas frecuencias,” in *Latinmag 2019*, Dec 2019. [Online]. Available: https://www.elatinmag.com/aplimetodos-103-trench

[7] L. M. Carducci, R. Alonso, F. Luna, J. Zola, E. Zothner, and W. G. Fano, “Aplicaciones y métodos de medición y procesamiento de señales para la detección de anomalías de campo magnético de muy bajas frecuencias,” *LATINMAG 2019*, 2019.

[8] E. Maffia, V. Trainotti, W. G. Fano, and N. Trench, “Medición de la resonancia de Schumann,” *Latinmag Letter*, vol. 1, no. A02, pp. 1–8, 2011.

[9] G. T. et al, “Design and implementation of a test fixture for ELF Schumann resonance magnetic antenna receiver and magnetic permeability measurements,” *Electronics, 2020, 9, 171*, 2020.